AIChE

Evaluation of Mixed-Conducting Lanthanum-Strontium-Cobaltite Ceramic Membrane for Oxygen Separation

Lei Ge, Zongping Shao, Kun Zhang, and Ran Ran
State Key Laboratory of Materials-Oriented Chemical Engineering, Nanjing University of Technology, Nanjing 210009, P.R. China

J. C. Diniz da Costa and Shaomin Liu
FimLab-Films and Inorganic Membrane Laboratory, Div. of Chemical Engineering, University of Queensland, Queensland, Australia

DOI 10.1002/aic.11857
Published online July 23, 2009 in Wiley InterScience (www.interscience.wiley.com).

In this study, $La_{0.4}Sr_{0.6}CoO_{3-\delta}$ (LSC) oxide was synthesized via an EDTA-citrate complexing process and its application as a mixed-conducting ceramic membrane for oxygen separation was systematically investigated. The phase structure of the powder and microstructure of the membrane were characterized by XRD and SEM, respectively. The optimum condition for membrane sintering was developed based on SEM and four-probe DC electrical conductivity characterizations. The oxygen permeation fluxes at various temperatures and oxygen partial pressure gradients were measured by gas chromatography method. Fundamental equations of oxygen permeation and transport resistance through mixed conducting membrane were developed. The oxygen bulk diffusion coefficient (D_v) and surface exchange coefficient (K_{ex}) for LSC membrane were derived by model regression. The importance of surface exchange kinetics at each side of the membrane on oxygen permeation flux under different oxygen partial pressure gradients and temperatures were quantitatively distinguished from the oxygen bulk diffusion. The maximum oxygen flux achieved based on 1.6-mm-thick $La_{0.4}Sr_{0.6}CoO_{3-\delta}$ membrane was $\sim 4.0 \times 10^{-7}$ mol cm^{-2} s^{-1} at 950°C. However, calculation results show theoretical oxygen fluxes as high as 2.98×10^{-5} mol cm^{-2} s^{-1} through a 5-μm-thick LSC membrane with ideal surface modification when operating at 950°C for air separation. *AIChE J,* 55: 2603–2613, 2009
Keywords: $La_{0.4}Sr_{0.6}CoO_{3-\delta}$, ceramic membrane, oxygen separation, rate determination

Introduction

Dense ceramic membranes made from mixed ionic and electronic conducting (MIEC) oxides have recently attracted considerable attention not only from research community but also from industrial companies because of their potential applications in air separation and high-temperature membrane reactors for partial oxidations of light hydrocarbons.[1–10] Among various MIEC ceramics, perovskite-type oxides $(La,Sr)(Co,Fe)O_{3-\delta}$ were proven to be promising materials for oxygen separation membranes, membrane reactors, and cathodes of solid-oxide fuel cells.[11–18] These oxides usually have overwhelming electronic conductivity, although the oxygen-ionic conductivity could still be several orders of

Correspondence concerning this article should be addressed to Z. Shao at shaozp@njut.edu.cn or S. Liu at shaomin.liu@curtin.edu.au

magnitude higher than that of typical solid-oxide electrolytes of yttria-stabilized zirconia. The oxygen permeation fluxes of the corresponding membranes are generally closely related with the oxygen-ionic conductivity of the materials. In particular, the $La_{1-x}Sr_xCoO_{3-\delta}$-based perovskites exhibited not only high electronic/ionic conductivity but also high surface oxygen exchange kinetics.[19–21] These excellent properties make $La_{1-x}Sr_xCoO_{3-\delta}$ ideal materials for surface coating to improve oxygen surface exchange kinetics.[21] Recently, more fundamental understanding on the oxygen ionic conducting mechanism of $La_{1-x}Sr_xCoO_{3-\delta}$ oxides has been proposed by using newly developed experimental techniques such as transient TG technique, XPS spectra, isotope exchange technique, electrical relaxation, and volumetric titration method.[22–26] However, the systematic investigation of oxygen permeation behavior through $La_{0.4}Sr_{0.6}CoO_{3-\delta}$ membranes for air separation has yet to be realized.

Under the driving force of oxygen gradient, oxygen will permeate through dense MIEC membranes from the high-pressure side to the oxygen lean pressure side. The permeation process can be simply separated to three main stages: (1) oxygen transfer from the gas phase to the membrane surface, physical adsorption on surface, dissociation with electronic transfer to yield chemisorbed oxygen species, and the incorporation in surface layer; (2) ambipolar conductivity: oxygen ionic and electronic transport in opposite direction under an oxygen chemical potential gradient; and (3) the desorption of oxygen in the side of lower oxygen partial pressure. Oxygen vacancy diffusion coefficient (D_v) and surface exchange coefficient (K_{ex}) are two basic parameters quantitatively determining the permeation process. D_v and K_{ex} can be identified by proper fitting of the oxygen fluxes under different conditions. Clarification of the rate-determination steps of oxygen permeation through the membranes is important for the optimization of operation condition and further development of new materials.

In this study, the oxygen permeation behavior of one particular composition of $La_xSr_{1-x}CoO_{3-\delta}$, i.e., $La_{0.4}Sr_{0.6}CoO_{3-\delta}$ (LSC) membrane, was investigated both theoretically and experimentally. D_v and K_{ex} and membrane characteristic thickness were calculated by the application of the developed models. The roles of surface exchanges and bulk diffusion in the overall performance of LSC membrane for oxygen permeation were discussed. The oxygen permeation polarization resistances were identified to clarify the rate-limiting steps.

Theory

Oxygen fluxes in the mixed conducting membranes

Based on the Nerst-Planck equation combining Fick's law and ion migration, the fluxes of charged defects in mixed conducting membranes at steady state under the electrochemical potential gradient is expressed in Eq. 1[27–29]:

$$J_i = -D_i C_i \left[\frac{1 - t_i}{C_i} \cdot \frac{dC_i}{dL} - \sum_{j=i} \frac{z_i}{z_j} \cdot \frac{t_i}{C_i} \cdot \frac{dC_j}{dL} \right] \tag{1}$$

where D, C, z, t, L are the diffusivity, concentration, charge number, and the transport number of defect i, and membrane thickness, respectively. When the oxygen vacancy ($V_{\dot{O}}^{\bullet\bullet}$) and electron hole ($\dot{h}$) are the only mobile charged carriers in the mixed conducting membranes,[30] which are true for many MIEC perovskite oxides under relatively high oxygen partial pressure of the surrounding atmospheres, and then Eq. 1 can be simplified to

$$J_V = -\frac{(C_h + 4C_V)D_v D_h}{C_h D_h + 4C_V D_v} \cdot \frac{dC_V}{dL} \tag{2}$$

If the ionic transference number is very small ($C_h D_h >> C_V D_v$ and $C_h >> C_V$), it is true for many MIEC perovskite oxides, Eq. 2 can be further simplified to

$$J_V = -D_v \cdot \frac{dC_V}{dL} \tag{3}$$

Based on the stoichiometric relations of oxygen and the oxygen vacancy, the oxygen flux can be written as

$$J_{O_2} = -\frac{1}{2} J_V = \frac{D_v}{2} \cdot \frac{dC_V}{dL} \tag{4}$$

Before further theoretical derivation, two of the most important parameters, diffusion coefficient (D_v) and surface coefficient (k or K), need to be clarified. They are considered to be a constant at a given temperature, independent of membrane thickness and gas flow rates or pressures, but dependent on temperature and material properties. Surface coefficients (k or K) are also dependent on membrane surface microstructure or morphologies.[28,31]

Because D_v is a constant at a temperature, the oxygen flux can be obtained by the integration of Eq. 4:

$$J_{O_2} = \frac{D_v}{2L} (C_V''^s - C_V'^s) \tag{5}$$

where C_V' and C_V'' are the steady-state oxygen vacancy concentrations at the high and low oxygen pressure sides of the membranes, respectively.

The oxygen vacancy concentrations on both membrane surfaces in Eq. 5 are also governed by surface exchange reactions. The surface oxygen exchange reaction between oxide surfaces and the gas phases is a multistep process, although it can be simply explained by two elementary steps as follows[31,32]:

$$\frac{1}{2} O_2 + V_O^{\bullet\bullet} \underset{k_d}{\overset{k_a}{\rightleftarrows}} O_O^x + 2h^{\bullet} \tag{A}$$

$$O_O^x + 2h^{\bullet} \underset{k_a}{\overset{k_d}{\rightleftarrows}} \frac{1}{2} O_2 + V_O^{\bullet\bullet} \tag{B}$$

Reactions A and B are taking place in membrane surfaces-I (feed side) and II (sweep side), respectively. O_O^x represents the lattice oxygen in the perovskite crystal structure, and k_a, k_d are the forward and reverse reaction rate constants for the surface reactions, respectively. It is important to note that the electron holes are essentially constant at both surfaces of the membrane due to the high electronic conductivity, and thus the reverse and forward surface reaction rates are

pseudo zero-order at steady state under isothermal conditions. Therefore, the oxygen consummation or formation rate in the membrane surfaces can be expressed by:

$$J_{O_2} = k_a \cdot C_V^{'s} \cdot P_{O_2}^{'0.5} - k_d \tag{6a}$$

$$J_{O_2} = k_d - k_a C_V^{''s} \cdot P_{O_{''2}}^{0.5} \tag{6b}$$

where P'_{O_2} and P''_{O_2} are the partial pressures of oxygen at the feed side and permeate side, respectively. When both surfaces of the membrane are exposed to the atmospheres with the same oxygen partial pressure ($P'_{O_2} = P''_{O_2}$), there is no oxygen gradient (or driving force) across the membrane and the net flux through the surface is zero ($J_{O_2} = 0$). Equation 6 can be converted to:

$$k_a C_V^{'e} P_{O_2}^{'0.5} = k_a C_V^{''e} P''^{0.5}_{O_2} = k_d \tag{7}$$

where C'^{e}_{V} and C''^{e}_{V} are the oxygen vacancy concentrations in the material under thermal equilibrium with the atmosphere surrounded by P'_{O_2} and P''_{O_2}, respectively.

Under steady state, the oxygen fluxes at the both membrane surfaces and the bulk should be equal. Combining Eqs. 5–7, the oxygen permeation flux with the controlling steps of surface exchange kinetics and bulk diffusion can be expressed as follows:

$$J_{O_2} = k_a \, C_V^{'s} \, P'^{0.5}_{O_2} - k_a C_V^{'e} P'^{0.5}_{O_2} \tag{8}$$

$$J_{O_2} = k_a C_V^{''e} P''^{0.5}_{O_2} - k_a C_V^{''s} \, P''^{0.5}_{O_2} \tag{9}$$

Solving Eqs. 4, 8, and 9 simultaneously, it gives the oxygen flux as shown in Eq. 10:

$$J_{O_2} = \frac{D_v}{2L} \cdot \frac{\frac{k_a}{\frac{1}{P'^{0.5}_{O_2}} + \frac{1}{P''^{0.5}_{O_2}}}}{\frac{k_a}{\frac{1}{P'^{0.5}_{O_2}} + \frac{1}{P''^{0.5}_{O_2}}} + \frac{D_v}{2L}} \cdot (C_V^{''e} - C_V^{'e}) \tag{10}$$

Finally, D_v and k_a can be determined by proper fitting of the experimental data into Eq. 10, which requires prior knowledge of (i) C'^{e}_{V} and C''^{e}_{V} values and (ii) the oxygen permeation fluxes under the applied oxygen partial pressure gradient across the membrane ($P'_{O_2} - P''_{O_2}$) at selected temperatures by oxygen permeation experiments.

Surface exchange coefficients, characteristic thickness, and oxygen transport resistance

Membrane surface exchange coefficient at the feed side (K'_{ex}), surface exchange coefficient at the permeate side (K''_{ex}), and the overall surface exchange coefficient (K_{ex}) can be defined as follows:

$$K'_{ex} = k_a P'^{0.5}_{O_2} \tag{11}$$

$$K''_{ex} = k_a P''^{0.5}_{O_2} \tag{12}$$

$$K_{ex} = \frac{1}{\frac{1}{K'_{ex}} + \frac{1}{K''_{ex}}} = \frac{k_a}{\frac{1}{P'^{0.5}_{O_2}} + \frac{1}{P''^{0.5}_{O_2}}} \tag{13}$$

By introducing the surface exchange coefficients, the oxygen flux in Eq. 10 can be rewritten as

$$J_{O_2} = \frac{(C_V^{''e} - C_V^{'e})}{\frac{2L}{D_v} + \frac{1}{K_{ex}}} = \frac{\text{Driving force}}{\text{Diffusion resistance} + \text{Surface reaction resistance}} \tag{14}$$

When K_{ex} is far greater than $\frac{D_v}{2L}$ in case of ideal surface modification, the surface reaction will not exert any resistance to the oxygen permeation. The oxygen fluxes in Eq. 10 can also be written as follows:

$$J_{O_2} = \frac{D_v}{2L} \cdot (C_V^{''e} - C_V^{'e}) \tag{14a}$$

It should be noted that Eq. 14a can also be derived by the application of Wagner theory.

Another extreme situation lies in the case that K_{ex} is far less than $\frac{D_v}{2L}$. When the membrane is ultra thin and places little resistances, the permeation rate will largely be controlled by the surface reactions and the oxygen fluxes can be described as in Eq. 14b:

$$J_{O_2} = K_{ex} \cdot (C_V^{''e} - C_V^{'e}) \tag{14b}$$

At the condition of $K_{ex} = \frac{D_v}{2L}$, the surface exchange process and bulk oxygen diffusion process give equal resistance to the oxygen permeation through the membrane. The membrane thickness at this condition is defined as characteristic thickness,[33,34]

$$L_c = \frac{D_v}{2 \cdot k_a} \left(\frac{1}{P''^{0.5}_{O_2}} + \frac{1}{P'^{0.5}_{O_2}}\right) \tag{15}$$

L_c is obviously dependent on the membrane material properties (i.e., D_v and k_a) and membrane operating conditions (i.e., gas atmosphere and temperature). The membranes with higher D_v and operating at lower temperature or lower oxygen partial pressure environment would encounter a larger characteristic thickness. Based on TG results, the oxygen vacancy concentration in the equilibrium of C'^{e}_{V} and C''^{e}_{V} on both membrane sides can be calculated, and then the values of D and K were calculated by Eq. 10, which further derives the respective transport resistances based on the assumption that the linear kinetics are applicable for both the surface reactions and the bulk diffusion. It should be noted that SOFC electrodes often exhibit linear kinetics even under weak polarization.[35] The same idea of using the data of D_v and k_a to infer the permeation resistance was previously verified by other researchers.[32]

The overall driving force (chemical potential difference) and the oxygen transport polarization resistance[36] can be expressed in the following two equations:

$$E = -\frac{RT}{4F} \ln\left\{\frac{P''_{O_2}}{P'_{O_2}}\right\} = -\frac{RT}{4Fn} \ln\left\{\frac{C''^{e}_{V}}{C'^{e}_{V}}\right\} \tag{16}$$

$$R_{total} = -\frac{RT}{4^2F^2} \frac{1}{SJ_{O_2}} \ln\left\{\frac{P''_{O_2}}{P'_{O_2}}\right\} \tag{17}$$

where S is the effective surface membrane area.

The driving force lost over both surfaces (s_1 and s_2) sides of the membrane and the oxygen bulk diffusion can be calculated according to

$$\eta_{s_1} = -\frac{RT}{4F}\ln\left\{\frac{P'^{s}_{O_2}}{P'_{O_2}}\right\} = -\frac{RT}{4Fn}\ln\left\{\frac{C'^{s}_{V}}{C'^{e}_{V}}\right\} \quad (18)$$

$$\eta_{s_2} = -\frac{RT}{4F}\ln\left\{\frac{P''_{O_2}}{P''^{s}_{O_2}}\right\} = -\frac{RT}{4Fn}\ln\left\{\frac{C''^{e}_{V}}{C''^{s}_{V}}\right\} \quad (19)$$

$$\eta_{bulk} = -\frac{RT}{4F}\ln\left\{\frac{P''^{s}_{O_2}}{P^{s}_{O_{/2}}}\right\} = -\frac{RT}{4Fn}\ln\left\{\frac{C''^{s}_{V}}{C'^{s}_{V}}\right\} \quad (20)$$

By the same token, Eqs. 18–20 can be rearranged as oxygen transport resistances as follows:

$$R_{S_1} = R_{total}\cdot\frac{\eta_{S_1}}{E} = \frac{RT}{4^2F^2}\cdot\frac{1}{SJ_{O_2}}\cdot\ln\left\{\frac{P''_{O_2}}{P'_{O_2}}\right\}\cdot\frac{\ln\left\{\frac{C'^{s}_{V}}{C'^{e}_{V}}\right\}}{\ln\left\{\frac{C''^{e}_{V}}{C'^{e}_{V}}\right\}} \quad (21)$$

$$R_{S_2} = R_{total}\cdot\frac{\eta_{S_2}}{E} = \frac{RT}{4^2F^2}\cdot\frac{1}{SJ_{O_2}}\cdot\ln\left\{\frac{P''_{O_2}}{P'_{O_2}}\right\}\cdot\frac{\ln\left\{\frac{C''^{e}_{V}}{C''^{s}_{V}}\right\}}{\ln\left\{\frac{C''^{e}_{V}}{C'^{e}_{V}}\right\}} \quad (22)$$

$$R_{bulk} = R_{total}\cdot\frac{\eta_{bulk}}{E} = \frac{RT}{4^2F^2}\cdot\frac{1}{SJ_{O_2}}\cdot\ln\left\{\frac{P''_{O_2}}{P'_{O_2}}\right\}\cdot\frac{\ln\left\{\frac{C''^{s}_{V}}{C'^{s}_{V}}\right\}}{\ln\left\{\frac{C''^{e}_{V}}{C'^{e}_{V}}\right\}} \quad (23)$$

Experimental

Synthesis and preparation

Ceramic powders of LSC were synthesized via a combined EDTA-citrate complexing route.[37] Cobalt nitrate, lanthanum nitrate, and strontium nitrate, all in analytical grades, were used as the metal sources. EDTA powder and crystallized citric acid with purities higher than 99.5% were used as the chelating agents. After the calcination at 550–950°C for 5 h under stagnant air atmosphere, the powders were compacted into disk-shaped membranes using a stainless steel die (15 mm in diameter) under a hydraulic pressure of 20–40 tons. The disks were subsequently sintered at 1080–1230°C for 5 h. The final density of the membrane was estimated based on the SEM results. The membranes were tested prior to oxygen permeation measurements, and only gas-tight membranes were used for further experimental work.

Characterization

The crystal structure of the synthesized powders and membranes were characterized by X-ray diffraction (XRD, Bruker D8 Advance) using Cu Kα radiation ($\lambda = 1.5418$ Å). The experimental diffraction patterns were collected at room temperature by step scanning in the range of $20° \leq 2\theta \leq 80°$. The morphologies of the sintered membranes were examined using an environmental scanning electron microscope (QUANTA-2000).

The electrical conductivity was measured in oxygen, air, or argon atmospheres by four-probe DC method using Ag as electrodes upon cooling from 900 to 300°C, at 10°C per step.[36] The voltage response on the two voltage wires was recorded using a Keithley 2420 source meter with the current changed from 1 μA to 2 A. The conductivity was calculated based on the following equation:

$$\sigma = \frac{l}{A}\times K \quad (24)$$

where A is the cross-sectional area, l is the distance between the two voltage probes, and K is the slope of the curve of current vs. voltage.

Investigation of oxygen fluxes through LSC membranes was carried out by the gas chromatography (GC) method using a home-constructed high-temperature oxygen permeation reactor assembly described elsewhere.[38] Silver paste was used as the sealant to fix the membrane disk onto a dense quartz tube. The effective membrane surface area at the sweep side for permeation study was around 0.7 cm^2. The permeation cell was heated up to 950°C at the rate of 2°C min^{-1} to ensure an effective sealing. The oxygen partial pressure at the membrane feed side was stabilized at 0.21 atm (ambient air) unless otherwise specified. The helium was introduced to the sweep side chamber at a flow rate of 20–260 ml min^{-1} (STP). A HP 5890II gas chromatography equipped with a molecular sieve 5 Å molecular column was used to detect the gas concentrations. The oxygen partial pressure at the permeate side atmosphere was calculated by estimating oxygen concentration in effluent gas. The oxygen fluxes was calculated by

$$J_{O_2}(\text{mol cm}^{-2}\,\text{s}^{-1}) = \left[C_{O_2} - C_{N_2}\times\frac{0.21}{0.79}\times\left(\frac{28}{32}\right)^{\frac{1}{2}}\right]\times\frac{f}{S} \quad (25)$$

where C_O and C_N are the measured concentrations of oxygen and nitrogen in the gas on the sweep side (mol ml^{-1}), respectively, f is the flow rate of the exit gas on the sweep side (ml s^{-1}), and S is the membrane surface area of the sweep side (cm^2).

Results and Discussion

Phase structure and stability

The XRD pattern of as-prepared samples obtained after calcination at 550–950°C are given in Figure 1. Very weak diffraction peaks of rhombohedra perovskite phase in the sample calcined at 550°C was detected together with some impurities (i.e., $SrCO_3$, $SrCoO_{2.5}$). When the sintering temperature was elevated to 850°C, the powder was characterized by the crystal phase of LSC perovskite with all the diffraction peaks well indexed based on a rhombohedra structure. Because of the formation of thermally stable alkaline earth carbonate as the intermediate phase, the preparation of pure $La_{1-x}Sr_xCoO_{3-\delta}$ perovskite phase with high strontium content should be at temperatures higher than 900°C. However, too high sintering temperature may lead to undesirable crystallite growth and hard particle agglomerates. The prepared LSC powder calcined at 950°C displayed pure perovskite phase with appropriate grain size (35 nm) as estimated

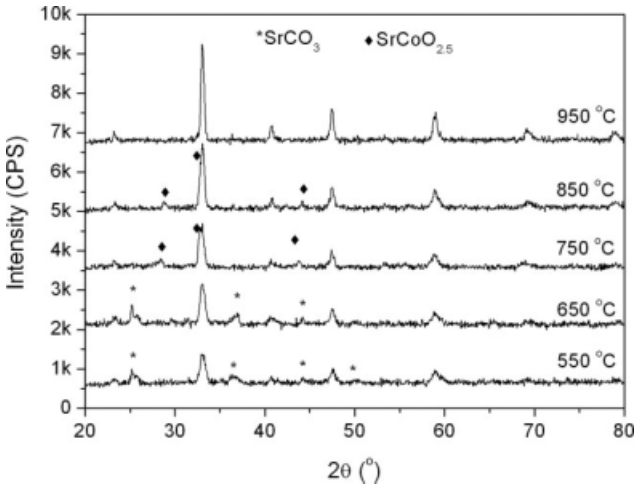

Figure 1. X-ray diffraction patterns of the as-prepared $La_{0.4}Sr_{0.6}CoO_{3-\delta}$ powder from calcination at varied temperatures.

by applying Scherrer's equation, and therefore was chosen as the ceramic membrane material in this work.

Figure 2 depicts the XRD patterns of the samples after annealed under various atmospheres (N_2, air, or O_2) for 10 h. It is observed that no phase structure changes occurred for all the samples. This clearly indicates that samples attained good stability in varying oxygen atmospheres from low to high concentrations, thus emulating similar conditions during oxygen permeation experiments. Good thermodynamic stability of $La_{1-x}Sr_xCoO_{3-\delta}$ ($x = 0$–0.8) oxides was also confirmed by DTA and high-temperature X-ray diffraction analysis in the temperature region from 597 to 997°C in Ref. 39.

Sintering behavior and electrical conductivity

Figure 3 shows the cross-sectional morphologies of the sintered membranes at various temperatures. A large quantity of pores with diameters of 1–5 μm was present in the membranes when sintered below 1080°C, as these conditions resulted in incomplete densification of the membranes. As the sintering temperature increased, the membrane became denser until reached 1180°C. The membrane deteriorated due to the material's melting behavior when the sintering temperature elevated to 1230°C.

The oxygen permeation flux was closely related with the transport number and electrical conductivity of the membrane. These mixed conducting perovskite oxides such as (La,Sr)(Co,Fe)$O_{3-\delta}$ or (Ba,Sr)(Co,Fe)$O_{3-\delta}$ usually have overwhelming electronic conductivity over the ionic conductivity.[11,16,36] The temperature dependence of the total conductivity of LSC is shown in Figure 4. The electronic conductivity in LSC system was dramatically higher than the ionic one, given an indication that measured conductivity mainly reflected the electronic conductivity. However, the electrical conductivity went down as temperature rose due to more oxygen vacancy formation. In the perovskite-related mixed conducting oxides, electron hopping through B-O-B bonds was realized via a mechanism like the Zener double exchange process.[40] The electron conduction was therefore hindered by the destruction of B-O-B bonds. Moreover, the electrical conductivity also increased as a function of the sintering temperature (1080–1180°C), which can be attributed to more densified structure of the membranes leading to the reduced grain boundary resistance (Figure 3). The phenomenon that ceramic membranes sintered at higher temperatures with less grain boundary area possessing higher conductivity was also observed from other perovskites like $La_{0.6}Sr_{0.4}Co_{0.2}Fe_{0.8}O_{3-\delta}$.[41]

Figure 5 illustrates the effects of oxygen concentration in the surrounding atmosphere of the membranes on the electrical conductivity of LSC measured by four-probe DC method. These results clearly show that the conductivity decreased with reducing oxygen partial pressures, which can be explained by the *p*-type electrical conducting mechanism. For *p*-type electrical conducting materials, the charge carrier is electron hole via surface reactions A or B. With the increase of oxygen partial pressure, the equilibrium of the reaction shifts to the right side, so the concentration of electron holes or electrical conductivity was increased.

Oxygen permeation properties

Oxygen Surface Exchange and Bulk Diffusion Coefficient. The oxygen permeation fluxes through LSC membrane ($L = 1.6$ mm) at various oxygen partial pressures of the oxygen lean side atmosphere and temperatures are shown in Figure 6. As can be seen, the membrane had high oxygen fluxes when operating at higher temperatures or lower oxygen partial pressures of the permeate side atmosphere. The parameters for permeation coefficient calculation in this work are summarized in Table 1. The bulk diffusion coefficient (D_v) and surface exchange coefficient (k_a) could be calculated using the slope and intercept from the linear relationship between $\frac{C''^e_V - C'^e_V}{J_{O_2}}$ and $\frac{1}{P'^{0.5}_{O_2}} + \frac{1}{P''^{0.5}_{O_2}}$. Figure 7 shows the calculated D_v and k_a at various temperatures and the effects of oxygen partial pressure in the permeate side on the overall surface exchange coefficients. Noteworthy is that the values of (D_v) of $La_{0.4}Sr_{0.6}CoO_{3-\delta}$ derived in this work were quite similar to $La_{0.3}Sr_{0.7}CoO_{3-\delta}$ perovskite via $^{18}O/^{16}O$ exchange

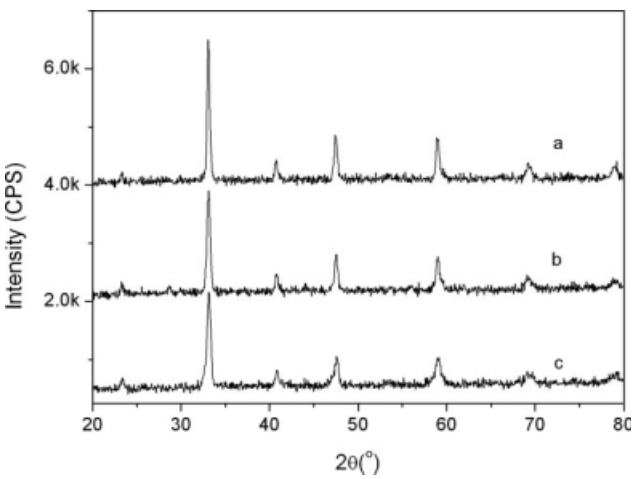

Figure 2. X-ray diffraction patterns of the sintered $La_{0.4}Sr_{0.6}CoO_{3-\delta}$ membranes after annealed under varied atmospheres at 850°C for 10 h.

a: O_2; b: air; c: N_2.

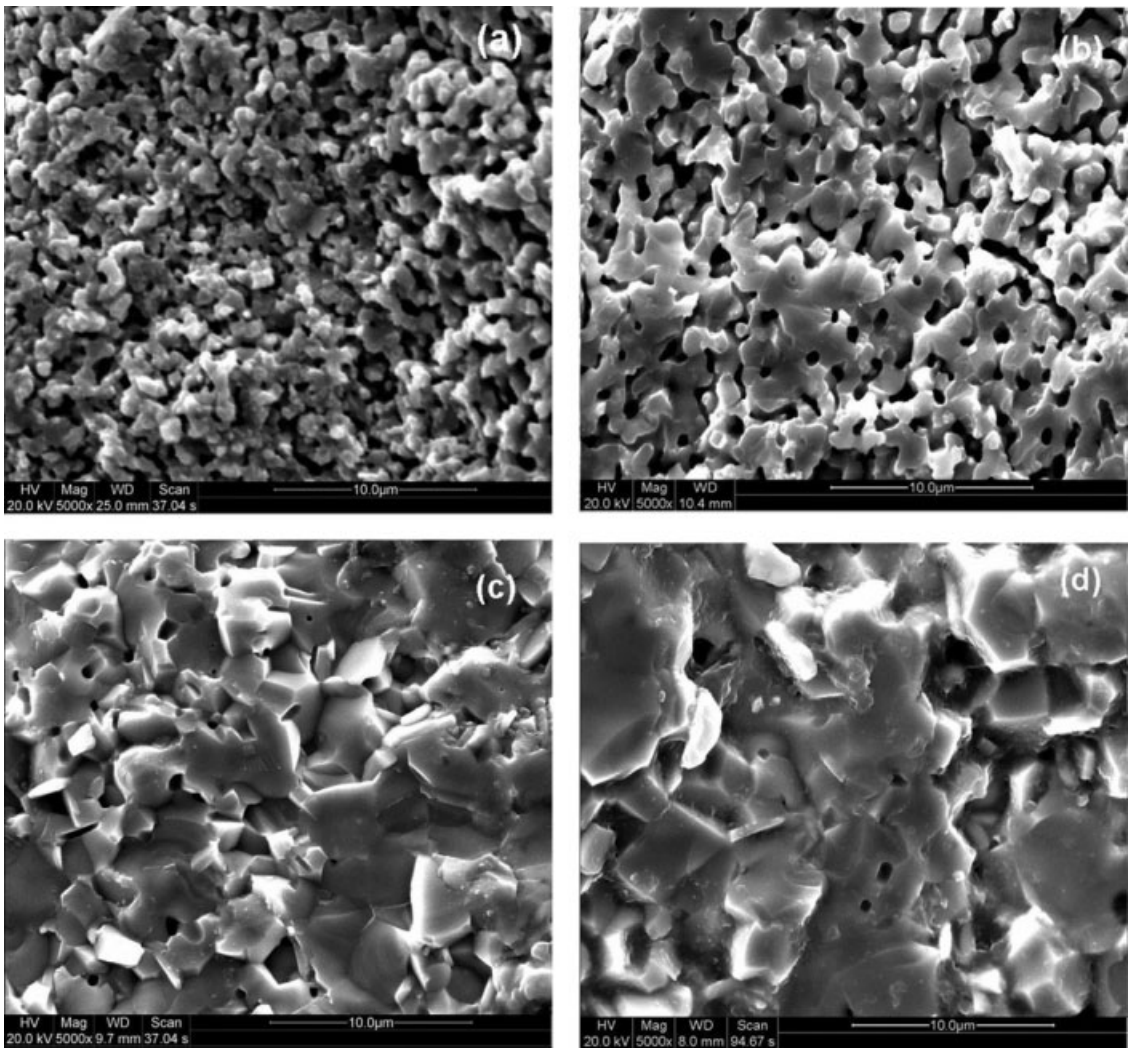

Figure 3. Cross-sectional morphologies of $La_{0.4}Sr_{0.6}CoO_{3-\delta}$ membranes sintered at varied temperatures.

a: 1080°C; b: 1130°C; c: 1180°C; d: 1230°C.

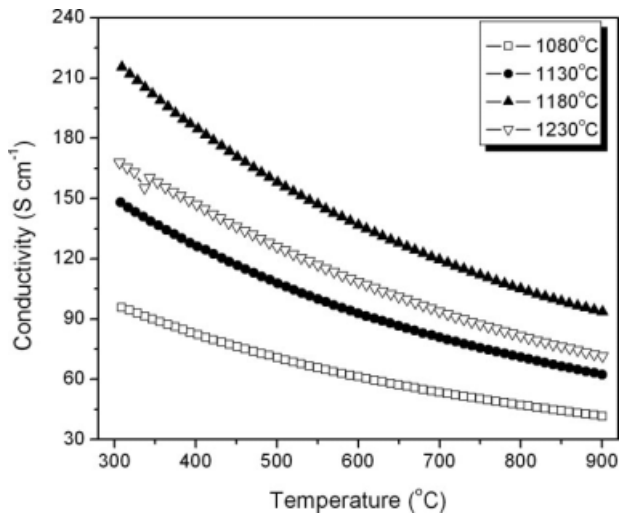

Figure 4. Temperature dependence of electrical conductivity of $La_{0.4}Sr_{0.6}CoO_{3-\delta}$ ceramics in air-sintered at varied temperatures.

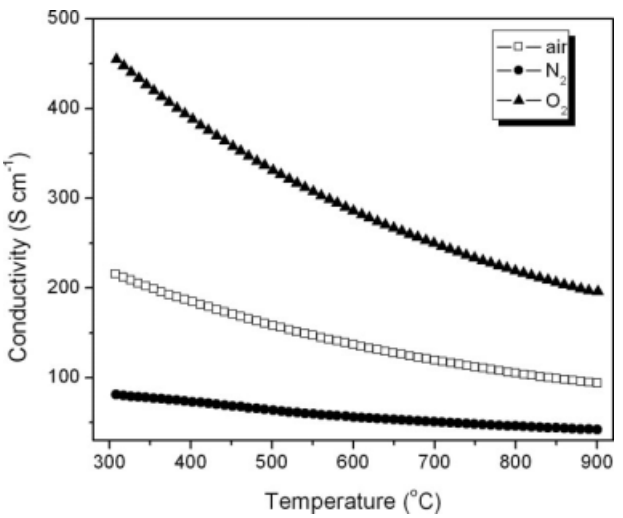

Figure 5. Electrical conductivity of $La_{0.4}Sr_{0.6}CoO_{3-\delta}$ under varied atmospheres.

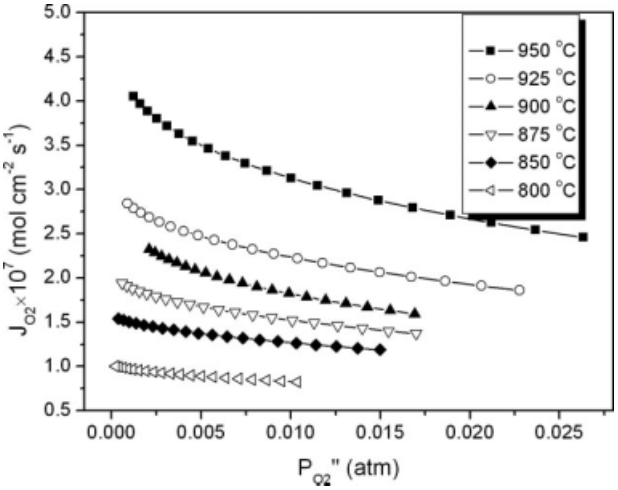

Figure 6. The lean side oxygen partial pressure dependence of oxygen permeation fluxes through $La_{0.4}Sr_{0.6}CoO_{3-\delta}$ membranes at various temperatures.

and dynamic SIMS analysis reported elsewhere.[42] One possible reason for this phenomenon is due to the similar material composition and phase structure between $La_{0.4}Sr_{0.6}CoO_{3-\delta}$ and $La_{0.3}Sr_{0.7}CoO_{3-\delta}$. Activation energies for oxygen surface exchange, bulk diffusion, and the overall oxygen permeation process determined via the Arrhenius equation were 82, 100, and 93.4 kJ mol^{-1}, respectively. Chen et al.[43] reported a lower value of around 60 kJ mol^{-1} for a $La_{0.3}Sr_{0.7}CoO_{3-\delta}$ membrane. The oxygen permeation process can be rate-determined by either the bulk oxygen diffusion or surface exchange kinetics, so the activation energy reflected the overall threshold energy to be overcome from these two limiting processes. The decrease of Sr-doping in $La_{1-x}Sr_xCoO_{3-\delta}$ may have led to the reduction of surface exchange and bulk diffusion rate, thus requiring higher activation energy for oxygen permeation.

Characteristic Thickness, Permeation Resistance, and Oxygen Fluxes

The characteristic thickness (L_c) is an important parameter that can be used to evaluate the roles that surface exchange

Table 1. Parameters for Theoretical Calculation

Pellet Membrane	$La_{0.4}Sr_{0.6}CoO_{3-\delta}$
Membrane thickness (L)	1.6 mm
The effective membrane surface area (S)	0.7 cm^2
Operating temperature (T)	800–950°C
Oxygen partial pressure at feed side (P'_{O_2})	0.21 atm
Oxygen partial pressure at sweep side (P''_{O_2})	0.0002–0.05 atm
Crystal volume (V_c)	55.75 Å^3
Mole volume (V_m)	33.56 cm^3 mol^{-1}
Oxygen nonstoichiometry (δ)	$\log\ \delta = A + B\log(P_{O_2})$[42] 950°C: $A = -0.6394$, $B = -0.0633$ 900°C: $A = -0.6556$, $B = -0.0623$ 850°C: $A = -0.6915$, $B = -0.0661$
Oxygen vacancies concentrations (C_v)	δ/V_m, mol cm^{-3}

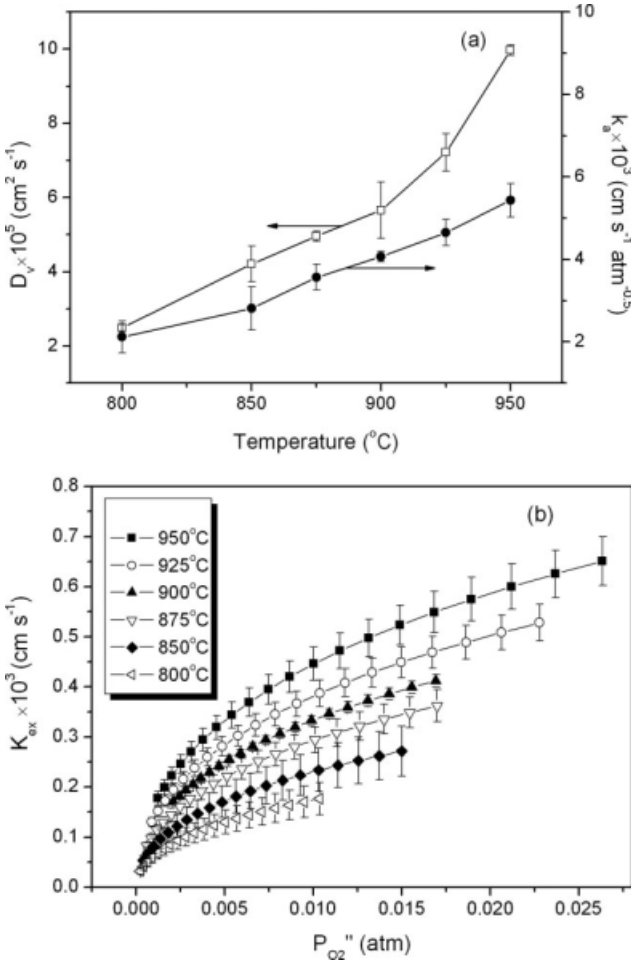

Figure 7. (a) Oxygen vacancy diffusion coefficient (D_v) and surface reaction coefficient (k_a); and (b) the overall surface exchange coefficient (K_{ex}) calculated from model derivation based on oxygen permeation fluxes of 1.6 mm $La_{0.4}Sr_{0.6}CoO_{3-\delta}$ membrane at various temperatures.

kinetics and bulk diffusion play in the oxygen permeation process. For example, when the membrane thickness is far less than L_c, the surface exchange reaction will become the rate-limiting step and the oxygen permeation rate can only be improved via surface modification. Figure 8 shows the L_c values of LSC at various operating conditions calculated by the application of Eq. 15. As shown in Figure 8, L_c ranged between 0.6 and 2.2 mm as a function of temperature (800–950°C) and oxygen partial pressure (0.002–0.21 atm). L_c increased by a higher operating temperature or lower oxygen partial pressure. In this work, the actual membrane thickness of 1.6 mm was quite close to the characteristic thickness L_c. As a consequence, both surface reactions and bulk diffusion imposed important influences on the oxygen permeation flux under the investigating temperature range or oxygen partial pressure range. The controlling steps can be further clarified by the analysis of the transport resistances over three main permeation steps.

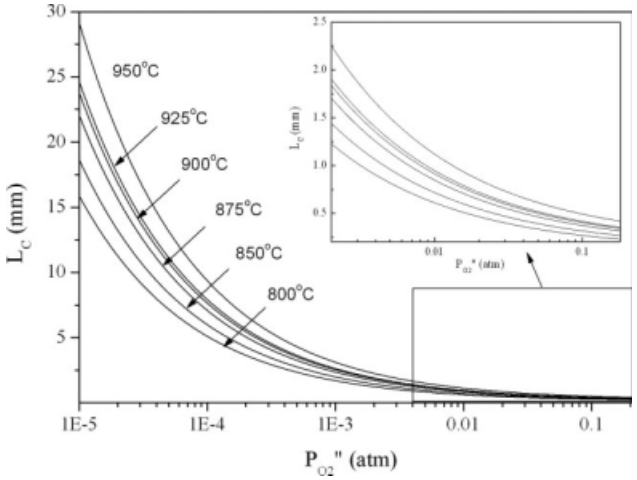

Figure 8. The lean side oxygen partial pressure (P''_{O_2}) dependence of characteristic membrane thickness (L_c) for oxygen permeation at various temperatures, P'_{O_2} = 0.21 atm.

The oxygen permeation polarization resistances at the membrane surfaces (R_{S1}, R_{S2}) and the bulk diffusion ohmic drop (R_{bulk}) together with the overall resistance (R_{total}) were quantitatively determined based on Eqs. 21–23. Figure 9 shows the effects of the oxygen partial pressure at the permeate side atmosphere (P''_{O_2}) on the resistances at 900°C. The partial pressure (P''_{O_2}) dependences of the four resistances (R_{S1}, R_{S2}, R_{bulk}, and R_{total}) at five temperatures that ranged from 800 to 950°C showed almost similar trend. As displayed in Figure 9, the surface resistance on the oxygen-rich side almost kept constant at all ranges of P''_{O_2} were investigated. The observation of this phenomenon was reasonable because the change of P''_{O_2} did not affect the gas atmosphere surrounding the membrane surface in the feed side. However, the change of P''_{O_2} did exert significant effect on the surface reaction resistance on the permeate side. As P''_{O_2} decreased by using a larger sweep gas rate, the resistance of R_{S2} increased sharply, which is consistent with the observations by Xu and Thomson.[32] For example, when P''_{O_2} decreased from 0.01 to 0.001 atm, R_{S2} values were increased from ~0.3 to ~0.7 Ω.

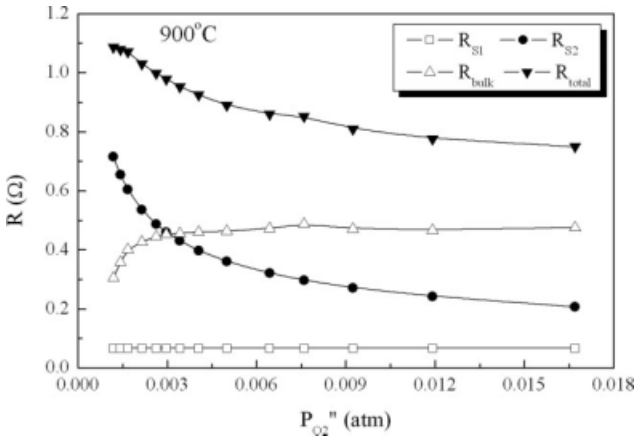

Figure 9. The lean side oxygen partial pressure (P''_{O_2}) dependence of various oxygen permeation resistances at 900°C, P'_{O_2} = 0.21 atm.

The effect of P''_{O_2} on the bulk diffusion ohmic resistance (R_{bulk}) can be explained as follows: the oxygen ion diffusion from membrane surface-I (feed side) to surface-II (permeate side) must comply with the oxygen vacancy diffusion in the opposite direction. According to Reaction B at membrane surface-II, a higher P''_{O_2} lowered the concentration of oxygen vacancies on the permeate side membrane surface or the oxygen vacancy concentration gradient, which are unfavorable to oxygen vacancy diffusion. This caused the oxygen diffusion to attain a larger resistance as discussed earlier. However, when P''_{O_2} was larger than 0.006 atm, the bulk diffusion resistance remained unchanged regardless of further increases of P''_{O_2}. Combining all the resistance changes, the overall oxygen permeation resistance was increased by a lower P''_{O_2} or by larger oxygen partial pressure gradient. Meanwhile, there was no significant differences between the total surface resistance and bulk resistance, suggesting again that the oxygen overall permeation rate was controlled by the mixed mode (i.e., both surface reaction and bulk diffusion). Moreover, in comparison of the two surface polarization resistances, the resistance in the permeate side was much larger than that on the oxygen feed side, indicating that the surface reaction on the permeate side played a more important role for oxygen permeation than the feed side. Similar results for other perovskites were reported elsewhere.[36] Under these circumstances, if membrane surface modification was carried out to improve the oxygen permeation rate, the modification is likely to be more beneficial on the surface of the membrane's permeate side rather than the feed side. In addition, this work also demonstrated that it was not effective to increase the oxygen fluxes by reducing the oxygen partial pressure to extremely low values in the permeate side due to the large increase of the overall permeation resistance. Figure 10 illustrates the temperature dependence on the resistances (R_{S1}, R_{S2}, R_{bulk}, and R_{total}) at the

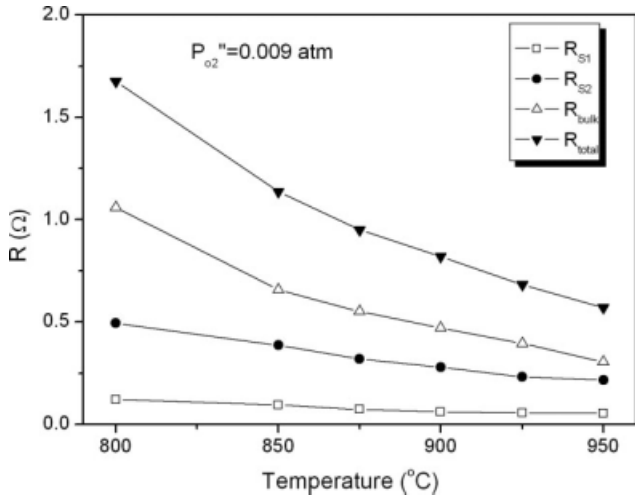

Figure 10. The temperature dependence of oxygen permeation polarization resistances through LSC membrane at P'_{O_2} = 0.21 atm and P''_{O_2} = 0.009 atm.

same oxygen partial pressure (P''_{O_2}) of 0.009 atm. As expected, all the resistances dropped as the temperature rose. Further inspection of the differences between these resistances reveals that at lower temperatures (800°C) bulk diffusion largely controlled the permeation process since the R_{bulk} was twofold of the surface reaction resistances. However, at high temperatures (950°C), the surface reaction resistance gradually equaled to the bulk diffusion resistance, thus clearly indicating their similar influences on the oxygen permeation flux.

Figure 11 shows the effects of thickness and the O_2 partial pressure (P''_{O_2}) in the permeate side on the oxygen fluxes through LSC membranes in two rate-controlling cases with one under the mixed bulk diffusion and surface exchange rates and another one only under bulk diffusion rate, which can be derived by the application of Eqs. 10 and 14a, respectively. According to oxygen permeation polarization resistance analysis, the reduction in membrane thickness and surface modification of the permeate side are required to further increase the oxygen fluxes through LSC membranes. In general, thinner thickness and larger partial oxygen gradient favor the oxygen fluxes. However, the permeation flux initially drops down with the decrease of oxygen partial pressure (P''_{O_2}) in the permeate side as can be seen from Figure 11a. This phenomenon can be reasonably explained by the analysis of the effect of oxygen partial pressure (P''_{O_2}) on the surface reaction resistance. As shown in Figure 9, the surface reaction resistance on the feed side increases dramatically due to the lowering of oxygen partial pressure (P''_{O_2}), which enlarges the total transportation resistance thus leading to a reducing permeation flux. Figure 11 can also be used to predict the oxygen fluxes at different conditions. For example, according to Figure 11a, operating at 850–950°C and the oxygen partial pressure at the permeate side around 10^{-5} to 10^{-6} atm, a 5-μm-thick membrane with similar surface morphology as membranes tested in this study could deliver an oxygen flux up to 3.57–8.46 $\times$ 10^{-6} mol cm^{-2} s^{-1}. When the membrane surfaces are ideally modified and the surface reaction exchange kinetics does not pose significant resistance, the oxygen permeation process was totally controlled by the relatively slow oxygen bulk diffusion. In this case, according to Figure 11b, the permeation flux will be significantly improved. For instance, the permeation flux of the 5-μm-thick membrane under same operating conditions (P''_{O_2} = 10^{-5} to 10^{-6} atm, 850–950°C) will be improved to 1.63–2.98 $\times$ 10^{-5} mol cm^{-2} s^{-1}. Therefore, the surface modification is essential for thin membranes to increase the permeation fluxes especially under low permeate side O_2 partial pressure. It should be mentioned that theoretical prediction from Figure 11b is quite consistent with the permeation results from other researchers with the material of $La_{0.3}Sr_{0.7}CoO_{3-\delta}$ by the application of Wagner's equation.[43]

It is reported that under the vacuum operation model, the oxygen partial pressure in the permeate side as low as 10^{-13} atm could be reached.[44] In this case, the fluxes would be extremely high. Because of the poor mechanical strength of thinner perovskite materials, such membrane systems in real application can be realized in asymmetric structure where the thin membranes are supported on porous substrates. Many thin film technologies such as mechanical copressing, tape casting, slurry coating, wet powder spray, electrochemical vapor deposition, and so on can be used to realize this purpose. However, it should be noted that the practical applications of perovskite membranes, such as fuel cell and gas separation, are often carried out in high-temperature environment where cracks of the composite membranes are, therefore, inevitable due to the mismatch of the thermal expansion between the different materials unless the membrane system is made from the same or similar materials.

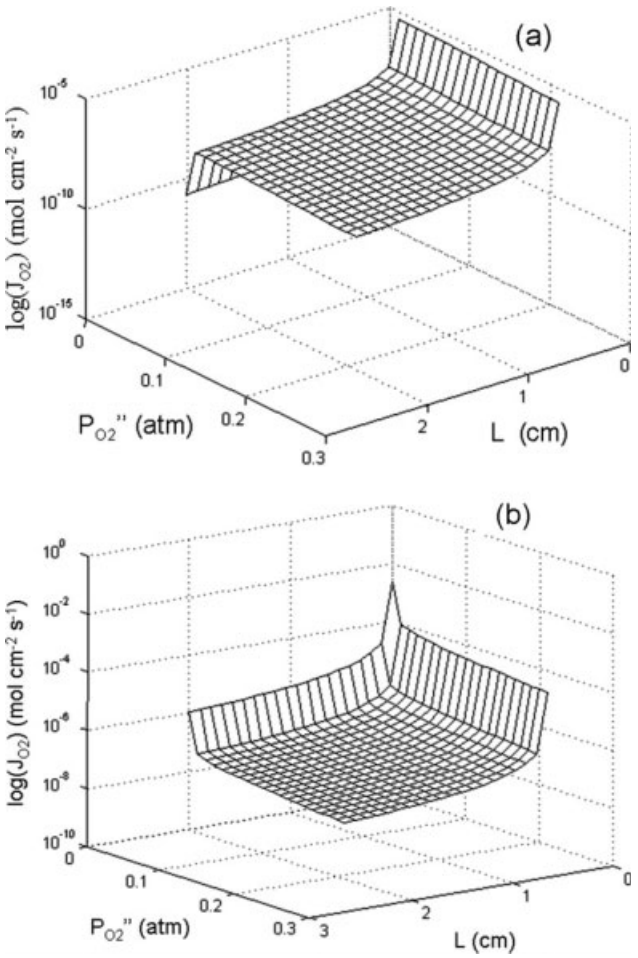

Figure 11. The thickness and lean side oxygen partial pressure (P''_{O_2}) dependence of oxygen permeation flux through $La_{0.4}Sr_{0.6}CoO_{3-\delta}$ membrane at a fixed oxygen partial pressure (P'_{O_2} = 0.21 atm) of the feed side atmosphere at 950°C.

(a) In mixed rate determination; (b) controlled by bulk diffusion with ideal surface modification.

Conclusions

In this work, $La_{0.4}Sr_{0.6}CoO_{3-\delta}$ perovskite oxide was synthesized via a complexing EDTA-citrate process followed by heat treatment at 950°C. The oxygen permeation was measured at different conditions. Mathematical models for the evaluation of oxygen permeation fluxes and resistances through the mixed conducting perovskites were developed,

which are more useful for the application in practical separating conditions where bulk diffusion and surface reactions jointly influence the oxygen permeation process. The derived oxygen surface exchange and bulk diffusion coefficients at 800–950°C ranged from 2.49–9.97 $\times 10^{-5}$ cm^2 s^{-1} to 2.12–5.43 $\times 10^{-3}$ cm s^{-1} atm$^{-0.5}$, respectively. The highest oxygen flux through the prepared disk-shaped $La_{0.4}Sr_{0.6}CoO_{3-\delta}$ membrane measured at 950°C was $\sim$4.0 $\times 10^{-7}$ mol cm^{-2} s^{-1} in this study. Theoretical analysis indicated that the oxygen permeation rate through $La_{0.4}Sr_{0.6}CoO_{3-\delta}$ disk-shaped membrane was controlled by both the bulk diffusion and oxygen surface reaction kinetics. In comparison of the two surface reaction resistances, the resistance in the permeate side was much larger than that on the feed oxygen-rich side. Membrane thickness reduction with surface modification was an effective method to further improve the oxygen permeation fluxes. The model simulated the performance of disk-shaped $La_{0.4}Sr_{0.6}CoO_{3-\delta}$ membranes with surface modification for air separation and oxygen permeation flux through a membrane thickness of 5 μm could reach up to 2.98 $\times 10^{-5}$ mol cm^{-2} s^{-1} at 950°C, respectively.

Acknowledgments

This work was supported by the National Natural Science Foundation of China, under contract nos. 20701020 and 20703024, Natural Science Foundation of Jiangsu Province, under contract no. BK2006180, by the National 863 program under contract no. 2007AA05Z133, and by the National Basic Research Program of China under contract no. 2007CB209704. Dr. Shaomin Liu acknowledges the ARC Fellowship provided by the Australian Research Council.

Notation

J_{O_2} = oxygen permeation flux, mol cm^{-2} s^{-1}
T = operating temperature, K
R = gas constant, 8.314 J mol^{-1} K^{-1}
F = Faraday constant, 96,500 C mol^{-1}
S = the effective membrane surface area, cm^2
σ_{total} = the sum of oxygen ionic conductivity and electronic conductivity, S cm^{-1}
σ_{ion} = oxygen ionic conductivity, S cm^{-1}
σ_e = electronic conductivity, S cm^{-1}
P'_{O_2} = oxygen partial pressure at the oxygen feed side atmosphere, atm
P''_{O_2} = oxygen partial pressure at the oxygen sweep side atmosphere, atm
$P'^{s}_{O_2}$ = oxygen partial pressure at the oxygen feed side membrane surface, atm
$P''^{s}_{O_2}$ = oxygen partial pressure at the oxygen sweep side membrane surface, atm
D_v = effective diffusivity of oxygen vacancy, cm^2 s^{-1}
C'^{s}_V = oxygen vacancies concentrations of high oxygen pressure sides of the membrane, mol cm^{-3}
C''^{s}_V = oxygen vacancies concentrations of low oxygen pressure sides of the membrane, mol cm^{-3}
C'^{e}_V = oxygen vacancies concentrations in the material under thermal equilibrium of high oxygen pressure sides of the membrane, mol cm^{-3}
C''^{e}_V = oxygen vacancies concentrations in the material under thermal equilibrium of low oxygen pressure sides of the membrane, mol cm^{-3}
C'_h = electron-holes concentrations of high oxygen pressure sides of the membrane, mol cm^{-3}
C''_h = electron-holes concentrations of low oxygen pressure sides of the membrane, mol cm^{-3}
K_{ex} = the overall surface exchange coefficient, cm s^{-1}
K'_{ex} = the surface exchange coefficient at the feed side membrane surface, cm s^{-1}
K''_{ex} = the surface exchange coefficient at the sweep side membrane surface, cm s^{-1}
L_c = characteristic membrane thickness, mm
E = the overall driving force, V
η_{s1} = the lost of driving force over the feed side membrane surface, V
η_{s2} = the lost of driving force over the sweep side membrane surface, V
η_{total} = the lost of driving force over the oxygen bulk diffusion, V
R_{total} = the overall oxygen transport resistance, Ω
R_{s1} = the resistances to surface oxygen exchange at high oxygen partial pressure side, Ω
R_{s2} = the resistances to surface oxygen exchange at low oxygen partial pressure side, Ω
R_{bulk} = the resistances to surface oxygen exchange at bulk, Ω

Literature Cited

1. Teraoka Y, Zhang H, Furukawa S, Yamazoe N. Oxygen permeation through perovskite-type oxides. *Chem Lett*. 1985;11:1743–1746.
2. ten Elshof JE, Bouwmeester HJM, Verweij H. Oxidative coupling of methane in a mixed-conducting perovskite membrane reactor. *Appl Catal A*. 1995;130:195–212.
3. Lin YS, Zeng Y. Catalytic properties of oxygen semipermeable perovskite-type ceramic membrane materials for oxidative coupling of methane. *J Catal*. 1996;164:220–231.
4. Kharton VV, Naumovich EN, Nikolaev AV. Materials of high-temperature electrochemical oxygen membranes. *J Membr Sci*. 1996; 111:149–157.
5. Balachandran U, Dusek JT, Maiya PS, Ma B, Mieville RL, Kleefisch MS, Udovich CA. Ceramic membrane reactor for converting methane to syngas. *Catal Today*. 1997;36:265–272.
6. Tsai CY, Dixon AG, Moser WR, Ma YH. Dense perovskite membrane reactors for partial oxidation of methane to syngas. *AIChE J*. 1997;43:2741–2750.
7. Ritchie JT, Richardson JT, Luss D. Ceramic membrane reactor for synthesis gas production. *AIChE J*. 2001;47:2092–2101.
8. Xu SJ, Thomson WJ. Perovskite-type oxide membranes for the oxidative coupling of methane. *AIChE J*. 1997;43:2731–2740.
9. Badwal SPS, Ciacchi FT. Ceramic membrane technologies for oxygen separation. *Adv Mater*. 2001;13:993–996.
10. Jin WQ, Zhang C, Zhang P, Fan YQ, Xu NP. Thermal decomposition of carbon dioxide coupled with POM in a membrane reactor. *AIChE J*. 2006;52:2545–2550.
11. Teraoka Y, Zhang H, Okamoto K, Yamazoe N. Mixed ionic-electronic conductivity of $La_{1-x}Sr_xCo_{1-y}Fe_yO_{3-d}$. *Mater Res Bull*. 1988; 23:51–58.
12. Zeng Y, Lin YS, Swartz SL. Perovskite-type ceramic membrane: synthesis, oxygen permeation and membrane reactor performance for oxidative coupling of methane. *J Membr Sci*. 1998;150:87–98.
13. Stevenson JW, Armstrong TR, Carnein RD, Pederson LR, Weber WJ. Electrochemical properties of mixed conducting perovskites, $La_{1-x}M_xCo_{1-y}Fe_yO_{3-d}$ (M=Sr, Ba, Ca). *J Electrochem Soc*. 1996; 143:2722–2729.
14. Li SG, Jin WQ, Xu NP, Shi J. Synthesis and oxygen permeation properties of $La_{0.2}Sr_{0.8}Co_{0.2}Fe_{0.8}O_{3-\delta}$ membranes. *Solid State Ionics*. 1999;124:161–170.
15. Steele BCH, Bae JM. Properties of $La_{0.6}Sr_{0.4}Co_{0.2}Fe_{0.8}O_{3-x}$ (LSCF) double layer cathodes on gadolinium-doped cerium oxide (CGO) electrolytes. II. Role of oxygen exchange and diffusion. *Solid State Ionics*. 1998;106:255–261.
16. Petric A, Huang P, Tietz F. Evaluation of La-Sr-Co-Fe-O perovskites for solid oxide fuel cells and gas separation membranes. *Solid State Ionics*. 2000;135:719–725.
17. Tai LW, Nasrallah MM, Anderson HU, Sparlin DM, Sehlin SR. Structure and electrical properties of $La_{1-x}Sr_xCo_{1-y}Fe_yO_3$. I. The system $La_{08}Sr_{02}Co_{1-y}Fe_yO_3$. *Solid State Ionics*. 1995;76:259–271.
18. Liu JB, Co AC, Paulson S, Birss VI. Oxygen reduction at sol–gel derived $La_{0.8}Sr_{0.2}Co_{0.8}Fe_{0.2}O_3$ cathodes. *Solid State Ionics*. 2006; 177:377–387.
19. van Doorn RHE, Burggraaf AJ. Structural aspects of the ionic conductivity of $La_{1-x}Sr_xCoO_{3-\delta}$. *Solid State Ionics*. 2000;128:65–78.

20. Takeda Y, Kanno R, Noda M, Tomida Y, Yamamoto O. Cathodic polarization phenomena of perovskite oxide electrodes with stabilized zirconia. *J Electrochem Soc*. 1987;134:2656–2661.
21. Lee S, Lee KS, Woo SK, Kim JW, Ishihara T, Kim DK. Oxygen-permeating property of $LaSrBFeO_3$ (B=Co, Ga) perovskite membrane surface-modified by $LaSrCoO_3$. *Solid State Ionics*. 2000; 158:287–296.
22. van Doorn RHE, Fullarton IC, de Souza RA, Kilner JA, Bouwmeester HJM, Burggraaf AJ. Surface oxygen exchange of $La_{0.3}Sr_{0.7}CoO_{3-\delta}$. *Solid State Ionics*. 1997;96:1–7.
23. van Doorn RHE, Bouwmeester HJM, Burggraaf AJ. Kinetic decomposition of $La_{0.3}Sr_{0.7}CoO_{3-\delta}$ perovskite membranes during oxygen permeation. *Solid State Ionics*. 1998;111:263–272.
24. Mizusaki J, Mima Y, Yamauchi S, Fueki K, Tagawa H. Nonstoichiometry of the perovskite-type oxides $La_{1-x}Sr_xCoO_{3-\delta}$. *J Solid State Chem*. 1989;80:102–111.
25. Sitte W, Bucher E, Benisek A, Preis W. Oxygen nonstoichiometry and ionic transport properties of $La_{0.4}Sr_{0.6}CoO_{3-\delta}$. *Spectrochim Acta A*. 2001;57:2071–2076.
26. Kishimoto H, Sakai N, Horita T, Yamaji K, Brito ME, Yokokawa H. Cation transport behavior in SOFC cathode materials of $La_{0.8}Sr_{0.2}CoO_3$ and $La_{0.8}Sr_{0.2}FeO_3$ with perovskite structure. *Solid State Ionics*. 2007;178:1317–1325.
27. Goto KS. *Solid State Electrochemistry and Its Applications to Sensors and Electronic Devices*. Elsevier: Amsterdam, 1988.
28. Tan XY, Li K. Modeling of air separation in a LSCF hollow-fiber membrane module. *AIChE J*. 2002;48:1469–1477.
29. Tan XY, Liu SM, Li K, Hughes R. Theoretical analysis of ion permeation through mixed conducting membranes and its application to dehydrogenation reactions. *Solid State Ionics*. 2000;138:149–159.
30. Bouwmeester HJM, Burggraaf AJ. *Dense ceramic membranes for oxygen separation*. In: Burggraaf AJ, Cot L, editors. *Fundamentals of Inorganic Membrane Science and Technology*. Elsevier, Amsterdam, 1996, 435–436.
31. Lin YS, Wang W, Han J. Oxygen permeation through thin mixed-conducting solids oxide membranes. *AIChE J*. 1994;40:786–798.
32. Xu SJ, Thomson WJ. Oxygen permeation rates through ion-conducting perovskite membranes. *Chem Eng Sci*. 1999;54:3839–3850.
33. Steele BCH. Interfacial reactions associated with ceramic ion transport membranes. *Solid State Ionics*. 1995;75:157–165.
34. Bouwmeester HJM, Kruidhof H, Burggraaf AJ. Importance of the surface exchange kinetics as rate limiting step in oxygen permeation through mixed-conducting oxides. *Solid State Ionics*. 1994;72:185–194.
35. van Heuvein FH, Bouwmeester HJM. Electrode properties of Sr-doped $LaMnO_3$ on yttria-stabilized zirconia. II. Electrode kinetics. *J Electrochem Soc*. 1997;144:134–140.
36. Zeng PY, Chen ZH, Zhou W, Gu HX, Shao ZP, Liu SM. Re-evaluation of $Ba_{0.5}Sr_{0.5}Co_{0.8}Fe_{0.2}O_{3-d}$ perovskite as oxygen semi-permeable membrane. *J Membr Sci*. 2007;291:148–156.
37. Zhou W, Shao ZP, Jin WQ. Synthesis of nanocrystalline conducting composite oxides based on a non-ion selective combined complexing process for functional applications. *J Alloy Compd*. 2006;426:368–374.
38. Ge L, Zhou W, Ran R, Liu SM, Shao ZP, Jin WQ, Xu NP. Properties and performance of A-site deficient $(Ba_{0.5}Sr_{0.5})_{1-x}Co_{0.8}Fe_{0.2}O_{3-\delta}$ ($x \leq 0.3$) for oxygen permeating membrane. *J Membr Sci*. 2007;306:318–328.
39. Kharton VV, Naumovich EN, Vecher AA, Nikolaev AV. Oxide ion conduction in solid solutions $Ln_{1-x}Sr_xCoO_{3-\delta}$(Ln = La, Pr, Nd). *J Solid State Chem*. 1995;120:128–136.
40. Zener C. Interaction between the d-shells in the transition metals. II. Ferromagnetic compounds of manganese with perovskite structure. *Phys Rev*. 1951;82:403–405.
41. Zeng PY, Ran R, Chen ZH, Gu HX, Shao ZP, Diniz da Costa JC, Liu SM. Significant effects of sintering temperature on the performance of $La_{0.6}Sr_{0.4}Co_{0.2}Fe_{0.8}O_{3-\delta}$ oxygen selective membranes. *J Membr Sci*. 2007;302:171–179.
42. Petrov AN, Cherepanov VA, Kononchuk OF, Gavrilova LY. Oxygen nonstoichiometry of $La_{1-x}Sr_xCoO_{3-\delta}$ ($0<x \leq 0.6$). *J Solid State Chem*. 1990;87:69–76.
43. Chen CH, Bouwmeester HJM, van Doorn RHE, Kruidhof H, Burggraaf AJ. Oxygen permeation of $La_{0.3}Sr_{0.7}CoO_{3-\delta}$. *Solid State Ionics*. 1997;98:7–13.
44. Han J, Xomeritakis G, Lin YS. Oxygen permeation through thin zirconia/yttria membranes prepared by EVD. *Solid State Ionics*. 1997;93:263–272.

Manuscript received Sept. 16, 2008, and revision received Jan. 6, 2009.